Catalysis Today 143 (2009) 108–114

Contents lists available at ScienceDirect

Catalysis Today

journal homepage: www.elsevier.com/locate/cattod

Hydrodesulfurization of dibenzothiophene and a SRGO on sulfide Ni(Co)Mo/Al_2O_3 catalysts. Effect of Ru and Pd promotion

R.M. Navarro [a,*], P. Castaño [b], M.C. Álvarez-Galván [a], B. Pawelec [a]

[a] Instituto de Catálisis y Petroleoquímica, CSIC, c/ Marie Curie 2, Cantoblanco, 28049 Madrid, Spain
[b] Universidad del País Vasco, Dpto. Ingeniería Química, Apartado 644, 48080 Bilbao, Spain

ARTICLE INFO

Article history:
Available online 2 October 2008

Keywords:
Ruthenium
Palladium
Hydrodesulfurization
Dibenzothiophene
SRGO

ABSTRACT

Commercial Ni(Co)Mo/γ–Al_2O_3 catalysts were modified by the addition of Pd and Ru in order to enhance their hydrogenation function as required for the simultaneous elimination of sulfur, nitrogen and aromatics from a gasoil. The ternary catalysts were prepared by wet impregnation of the commercial samples with Ru and Pd salt solutions. The oxide precursors were characterized by S_{BET}, TPR, XRD, XPS and IR of adsorbed pyridine. The catalysts were tested in their sulfided forms to evaluate their activity in the hydrodesulfurization (HDS) of dibenzothiophene (DBT) and in the hydrotreating (HDT) of a straight run gas oil (SRGO; 0.11, 0.55 and 1.16 wt% of *S*). Catalyst screening in the HDS of DBT showed that: (i) the presence of isolated RuS_2 phases located on the catalyst surface contributed to overall catalytic activity and improved the catalyst hydrogenation function, (ii) catalyst doping with Ru was more effective than its doping with Pd, (iii) maximum activity was obtained at a Ru loading of 0.5 wt%, (iv) the NiMo catalyst formulation was more effective than its CoMo counterpart, and (v) a life test (87 h) performed on the 0.5%Ru/NiMo catalyst showed that this catalyst was less prone to deactivation than the NiMo reference sample. In the hydrotreatment of a SRGO (*S* = 0.55 wt%), the sulfide 0.5%Ru/NiMo/Al_2O_3 catalyst proved to be more active in the HDS and HDA reactions than a commercial NiMo/Al_2O_3 one.

1. Introduction

The need to produce clean engine fuels [1,2] combined with the prospect of processing poor-quality petroleum feedstocks and the thermodynamic limitations of a classical Co(Ni)Mo(W)/γ–Al_2O_3 catalyst for simultaneous deep hydrodesulfurization (HDS) and hydrodearomatization (HDA) at high temperature operation [3] has simulated the synthesis of novel catalysts such as NEBULA® [4]. The unsupported NEBULA® catalysts, which were developed jointly by Akzo Nobel, Nippon Ketjen and Exxon Mobil and marketed in 2001 [4], proved to be much more active than the classical alumina-supported Co(Ni)Mo formulation, but they are also more expensive. Thus, the challenge remains to design novel cost-effective catalysts.

In order to reduce the thermodynamic limitations of a commercial Co(Ni)Mo/γ–Al_2O_3 catalyst at high temperature operation, one possibility consists in their doping with small amounts of Ru or Pd. Since only a small amount of promoter is needed for catalyst doping, the use of ternary Ru(Pd)–Ni(Co)Mo/Al_2O_3 formulation seems a good way of circumventing the barrier of the prohibitive cost of noble metals. The present work exploited this idea by doping commercial Ni(Co)Mo/γ–Al_2O_3 catalysts (HR-348 and KF-758) with Ru and Pd sulfides in order to enhance their hydrogenation properties.

The supported and unsupported Ru and Pd sulfides were effective in deep HDS [5]. The exceptional hydrodesulfurization (HDS) activity of the unsupported (bulk) Ru and Pd metal sulfides was confirmed for the HDS of dibenzothiophene (DBT) [6]. Several interesting hydrotreating properties have also been observed when RuS_2 was supported on alumina [7 and references within]. Their properties, the influence of synthesis methods, activation procedures and their correlation with catalytic response have recently been reviewed by De Los Reyes [7]. We have also reported the enhancement of hydrogenation in the HDS of DBT at 593 K on Pd–Mo/ASA and Ru–Mo/ASA catalysts with respect to Ni–Mo/ASA [8,9]. Cattenot et al. [10] investigated the possibility of creating a mixed decorated site (NiRu)MoS by varying the Ni/Ru atomic ratio in the calcined Ru–NiMo/Al_2O_3 catalysts. The promoting effect of ruthenium in the HDS of DBT and the hydrogenation of tetralin over sulfided Ru–NiMo/Al_2O_3 systems was explained by the authors as

* Corresponding author.
E-mail address: r.navarro@icp.csic.es (R.M. Navarro).

0920-5861/$ – see front matter © 2008 Elsevier B.V. All rights reserved.
doi:10.1016/j.cattod.2008.08.038

being due to the substitution of Ni atoms by Ru [10]. However, the poisoning effect of ruthenium was also reported when binary Ru–Mo/Al_2O_3 catalysts were calcined at 600 °C, prior to activation by sulfidation [11]. This appears to be related to the formation of Ru–O–Mo species which, after sulfidation, are less active in the desulfurization of thiophene than the individual ruthenium and molybdenum sulfides.

Contrary to binary systems, the studies on the use of noble metals as second promoter are scarce and their activities were tested mainly with model feeds [10,12–19]. However, it is of paramount importance to verify catalyst activity with the real feed when the competitive adsorption of different compounds on the active sites occurs. In particular, this is important for the evaluation of catalyst resistance to poisoning because it is known that both polycyclic aromatics and basic organonitrogen compounds present in the gasoil inhibit the HDS reaction [20].

In this work, commercial Ni(Co)Mo/γ–Al_2O_3 catalysts have been modified with Pd and Ru in order to enhance their hydrogenation function. The ternary catalysts were prepared by wet impregnation of the commercial samples with Ru and Pd salt solutions followed by very slow controlled drying and calcination in air, to avoid the formation of undesired Ru(Pd)–O–Mo phases. Catalyst screening has been performed in the reaction of hydrodesulfurization (HDS) of dibenzothiophene (DBT) and then, the most active catalysts have been tested in the hydrotreatment (HDT) of strength run gas oil (SRGO). The effect of promoter (Ru vs. Pd), catalyst base formulation (NiMo vs. CoMo), Ru-loading and two different feedstocks have been investigated. The physicochemical properties of the oxide precursors and spent catalysts have been evaluated by various techniques (S_{BET}, TPR, FTIR of adsorbed pyridine and XPS) in order to elucidate factors influencing the catalyst response.

2. Experimental

2.1. Catalyst preparation and characterization

The Ru and Pd promoted Ni(Co)Mo/γ–Al_2O_3 catalysts were prepared by impregnation of commercial NiMo/Al_2O_3 (HR-348; S_{BET} = 164 $m^2\ g^{-1}$; Mo, Ni, P loading of 10.7, 2.48 and 2.64 wt%, respectively) and CoMo/Al_2O_3 catalysts (KF-752, S_{BET} = 223 $m^2\ g^{-1}$; Mo, Co and P loading of 14.2, 3.8 and 0.83 wt%, respectively) with aqueous solution of $RuCl_3{\cdot}xH_2O$ (Johnson Matthey Ltd.) or $Pd(NO_3)_2{\cdot}2H_2O$ (Fluka) with concentrations needed for achieving nominal noble metal oxide contents of 0.5 and 1.0 wt%. Before impregnation, the catalyst base was crushed and pelletized to obtain a particle size of 0.25–0.32 mm for optimal diffusion control. Drying was performed using a slow heating ramp (0.6 °C min^{-1}) up to 100 °C and maintaining this temperature for 1 h. Finally, the precursors were calcined slowly raising the temperature from 100 °C to 420 °C (1.8 °C min^{-1}) and then isothermally calcined at this temperature for 2 h. The physicochemical properties of oxide precursors and spent catalysts were evaluated by a variety of techniques: S_{BET}, XRD, TPR, FTIR spectroscopy of adsorbed pyridine and XPS. The experimental details are reported elsewhere [21,22]. For XPS measurements, the Al 2p peak was taken as an internal pattern (BE at 74.5 eV) and the BE of the Ru $3d_{5/2}$ core level was estimated after deconvolution of the C 1s peak.

2.2. Catalytic activity

Catalysts were tested in a continuous high-pressure fixed-bed reactor. The composition of the model feed was 1 wt% of DBT dissolved in decalin. For all tests, 0.3 g of the catalyst was diluted with 0.5 g of SiC (both in the 0.25–0.3 mm particle size range). Prior to activity tests, the catalyst was dried under a N_2 flow at 673 K for 1 h, and then sulfided in a H_2:H_2S mixture (ratio 10:1) at 400 °C for 4 h. The experimental details are reported elsewhere [9,22]. The absence of any diffusion limitations was verified previously. The reaction conditions were: P = 3.0 MPa; T = 250–320 °C, H_2 flow rate = 7 l (STP)/h and LHSV = 35 h^{-1}. Liquid samples were analyzed by GC with FID (Varian chromatograph Model Star 3400 CX) equipped with DB-1 column. Total DBT conversion was calculated as DBT disappearance, after reaching steady state. The HDS and HYD selectivities for the HDS of DBT reaction were defined as (BP)/(CHB + BP) × 100 and (CHB)/(CHB + BP) × 100, respectively.

Table 1
Composition of SRGO

Composition	S (ppm)	S (wt%)	N (ppm)	Aromatics (vol%)
SRGO	11 660	1.16	430	27.5
Hexadecane/SRGO ratio = 1.2 [*L*(STP)/*L*]	5259	0.55	251	12.3
Hexadecane/SRGO ratio = 9.5 [*L*(STP)/*L*]	1105	0.11	45	1.8

After catalyst screening in the HDS of DBT, the selected samples were tested in the hydrotreating of a SRGO carried out in the same micro plant described above. The main composition of the feed employed is presented in Table 1. The activity measurements used 3 g of the catalyst diluted with 5 g of SiC (both with particle sizes in the range 0.25–0.3 mm). The catalyst drying, sulfidation and further purging with N_2 are the same as described above. Reaction conditions were: T = 280–360 °C; H_2 pressure = 3.0 MPa and LHSV = 2.2 h^{-1}. Liquid samples were analyzed by Varian chromatograph Model Star 3400 CX.

3. Results and discussion

3.1. Hydrodesulfurization of dibenzothiophene

Prior to catalyst screening in the HDS of DBT, the effect of H_2 pressure, reaction temperature and LHSV was studied to obtain the maximum yield of hydrogenation products. Considering the influence of H_2 pressure, tests at temperature 280 °C and LHSV 35 h^{-1} were performed for hydrogen pressure ranging from 0.5 to 3.0 MPa. The results are presented in Fig. 1. It is observed that HDS conversion increases with a rise in H_2 pressure from 0.5 to 1.5 MPa. A further increase in the H_2 pressure did not lead to an increase in HDS conversion. As expected, the selectivity toward HYD products (S_{HYD}) increased greatly with a rise in H_2 pressure reaching a maximum at 3 MPa of H_2 pressure. An increase in the S_{HYD} led to a simultaneous decrease in the S_{HDS}.

The influence of the LHSV on the performance of 0.5%Ru/NiMo catalyst was studied at 320 °C, H_2 pressure 3 MPa and LHSV varying in the range 35–118 h^{-1}. The results are presented in Fig. 2. As seen in this figure, both DBT conversion and selectivity toward HYD products strongly decreased with an increase of LHSV up to 77 h^{-1}, but only slightly thereafter. Thus, the selected LHSV value for the catalytic test was 35 h^{-1}. Finally, as expected, the study on the influence of reaction temperature on the DBT conversion over 0.5%Ru/NiMo catalyst showed that activity increases with increasing reaction temperature from 280 °C to 360 °C (data not shown here), but HYD selectivity decreases simultaneously, which agrees with thermodynamic calculations [3].

Fig. 3(a) compares the DBT conversion of all catalysts in reaction at 280 °C, P = 3 MPa and LHSV = 35 h^{-1}. As seen in this figure, the HDS activity of both NiMo/Al_2O_3 and CoMo/Al_2O_3 commercial catalysts was strongly affected by the incorporation of noble metals. The trend in catalytic activity in the alumina-supported

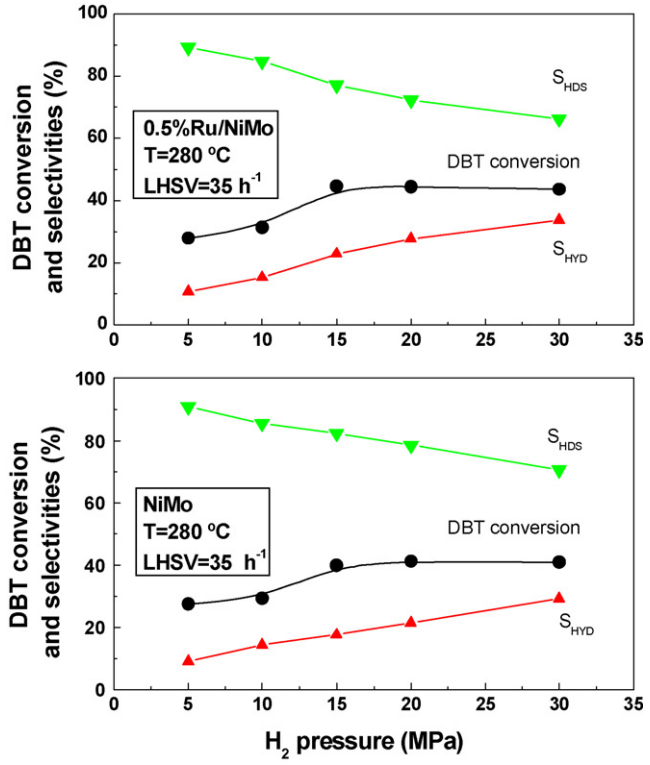

Fig. 1. Influence of the H_2 pressure in the HDS of DBT reaction over sulfided 0.5%Ru/NiMo and NiMo catalysts. Reaction conditions were: T = 280 °C, LHSV = 35 h^{-1} and H_2 = 0.5–3 MPa.

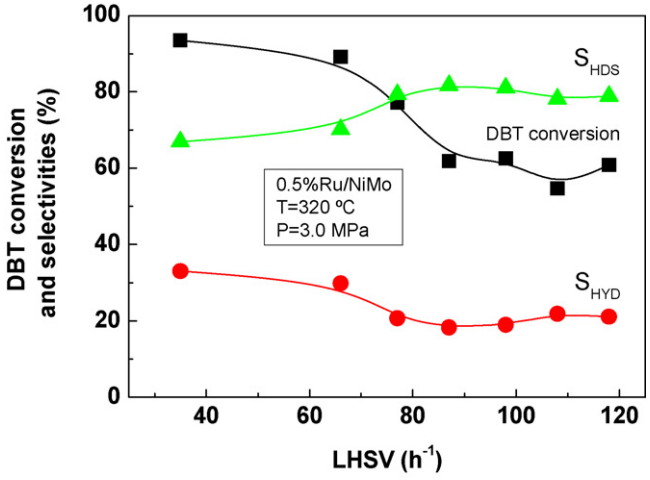

Fig. 2. Influence of the LHSV in the HDS of DBT reaction over sulfided 0.5%Ru/NiMo catalyst. Reaction conditions were: T = 320 °C, P = 3.0 MPa and LHSV = 35–118 h^{-1}.

catalysts follows the order: 1%Ru/NiNo > 1%Ru/CoMo > 0.5% Ru/NiMo > NiMo ≈ 1%Pd/NiMo > 0.5%Ru/CoMo > CoMo > 1%Pd/CoMo. In general, catalyst screening in the HDS of DBT under selected reaction conditions led us to conclude that: (i) the commercial NiMo catalyst was more active in the HDS of DBT than the commercial CoMo sample, in good agreement with a previous report [23], (ii) Ru is more effective as promoter than Pd, in good agreement with the activity profiles in the HDS of DBT on bulk transition metal sulfides [6] and (iii) the commercial NiMo/Al_2O_3 catalyst base recorded lower activity than its Ru-promoted NiMo/Al_2O_3 counterpart.

The compounds detected in the HDS of DBT were: unreached DBT, biphenyl (BP), cyclohexylbenzene (CHB) and traces of

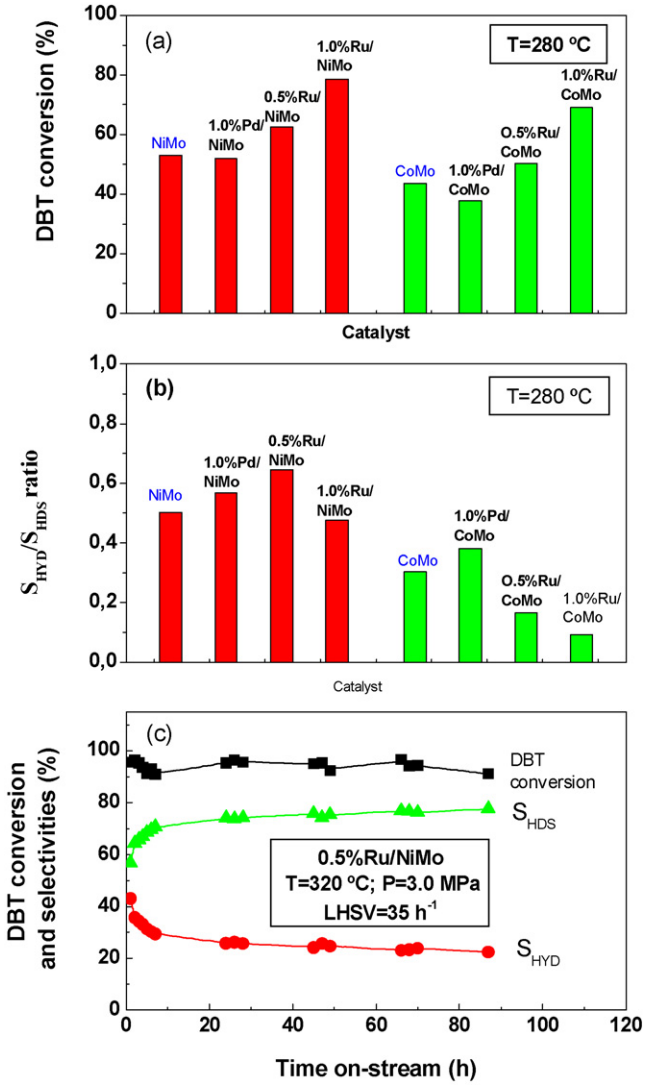

Fig. 3. HDS of DBT. (A) Effect of catalyst composition on the S removal (280 °C, 3 MPa), (B) effect of catalyst composition on the S_{HYD}/S_{HDS} selectivities ratio at (280 °C, 3 MPa), (C) and life test of the 0.5%Ru/NiMo catalyst (320 °C, 3 MPa).

tetrahydrodibenzothiophene (THDBT). BP and CHB were two major products of DBT conversion on all the catalysts studied; the former was produced *via* the direct desulfurization pathway (DDS), whereas the latter was formed from tetrahydrodibenzothiophene (THDBT) *via* this reaction's hydrogenation route (HYD). Fig. 3(b) compares the S_{HDS}/S_{HYD} selectivities ratio for all the catalysts studied in the HDS of DBT at T = 280 °C, P = 3 MPa, LHSV = 35 h^{-1} and steady-state conditions. According to this figure, the S_{HYD}/S_{HDS} selectivities ratio decreases in the following order: 0.5%Ru/NiMo > 1.0%Pd/NiMo > NiMo ≈ 1.0%Ru/NiMo > CoMo > 1.0%Pd/CoMo > 0.5%Ru/CoMo > 1.0%Ru/CoMo. For all catalysts, the S_{HYD}/S_{HDS} selectivity ratio was in the range 0.09–0.65. This indicates that the C–S bond cleavage reaction of DBT (formation of BP) is dominant over the hydrogenation of the aromatics ring, which agrees with previous findings [8,9]. As expected, the S_{HYD}/S_{HDS} selectivities ratios for the NiMo-based catalysts are always higher than their CoMo-based counterparts. This is because the NiMo catalyst base had almost twofold larger HYD properties than the CoMo catalyst base. We can note that the optimum Ru content is around 0.5 wt% (by higher S_{HYD}/S_{HDS} selectivities ratio) and this sample is 10% more active than the commercial NiMo catalyst

base (Fig. 3(a)). The catalyst life test showed that the 0.5%Ru/NiMo catalyst was stable during time-on stream of 87 h (Fig. 3(c)) whereas the 1.0%Ru/CoMo catalyst did not record deactivation during 50 h on-stream operation (data not shown here). The enhancement of the HYD capability of the 0.5%Ru/NiMo sample with respect to the NiMo catalyst base, as well as its longer catalyst life with respect to the 1.0%Ru/NiMo catalyst, makes it a good candidate for further study with real feed.

3.2. Hydrotreating of SRGO

Since the HDS of DBT test clearly indicated that the NiMo-based catalysts were more active than those based on the CoMo formulation, the former catalysts were selected for the activity test with a SRGO containing 1.16 wt% of S. As expected, the differences in activity between both Ru-promoted and unpromoted NiMo reference catalysts were less marked than in the tests with DBT. This points to a competitive adsorption of different reactive species over the catalyst surface under the reaction atmosphere, besides the fact that the reaction was performed in a down-flow reactor, which minimizes reaction inhibition due to the accumulation of H_2S in a reactor. In this sense, the significant retardation of the HDS reaction of 4,6-dimethyldibenzothiophene in the dominant presence of naphthalene over Ru–NiMo/Al_2O_3 catalysts was reported by Isoda et al. [16]. Interestingly, these authors found the smallest retardation of the HDS reaction by naphthalene when Co, Ru and Mo loadings were 0.25, 0.75 and 15 wt%, respectively.

The impact of the sulfur content in the SRGO (0.11, 0.55 and 1.16 wt%), in the HDS, HDN and HDA reactions over Ru-promoted and unpromoted NiMo catalysts, is shown in Fig. 4. As expected, the conversions of S- and N-containing compounds, as well as those of aromatics, decreased when raising S content in the feed. This decrease was lower for HDS than for HDN and HDA reactions. Surprisingly, irrespectively of the S-content in the feed, the Ru-promoted and unpromoted NiMo catalysts have the same catalytic response in the HDS reaction. However, the 0.5%Ru/NiMo catalyst showed, at medium S content (0.55 wt%), a ca. 20% higher HDN activity compared to that of industrial NiMo/Al_2O_3 and 1.0%Ru/NiMo catalysts. For the HDT of the SRGO containing 0.11 and 0.53 wt% of S, the 0.5%Ru/NiMo catalyst showed ca. 10% higher HDA activity than the NiMo reference sample.

Concerning the elimination of N-compounds, at high S content (1.16 wt%), the 1.0%Ru/NiMo catalyst showed lower activity compared to that of an industrial NiMo/Al_2O_3. In this case, it should be noted that the HDT of SRGO is carried out under high partial pressures of H_2S. Thus, in addition to inhibition phenomena, the H_2S environment could induce modifications to the structure of the 1.0%Ru/NiMo catalyst [7]. Finally, with the exception of the HDN, the catalytic response of the 1.0%Ru/NiMo catalyst was similar to those of the NiMo.

The influence of the reaction temperature on S-, N- and aromatics removal is shown in Fig. 5. The feed (SRGO) contains 0.55 wt% of sulfur, 251 ppm of nitrogen and 12.3 vol% of aromatics. As seen in Fig. 5, irrespectively of the reaction temperature, the 0.5%Ru/NiMo catalyst is the most active among the catalysts studied. For this catalyst, the maximum S, N and aromatics removal from gasoil was achieved at 320, 260 and 300 °C, respectively. Thus, for both the HDS of DBT and the HDT of SRGO, the optimized Ru loading is found to be 0.5 wt%.

3.3. Characterization of the oxide precursors

Irrespectively of the second promoter (Ru or Pd), the catalysts based on CoMo formulation show a larger S_{BET} than their

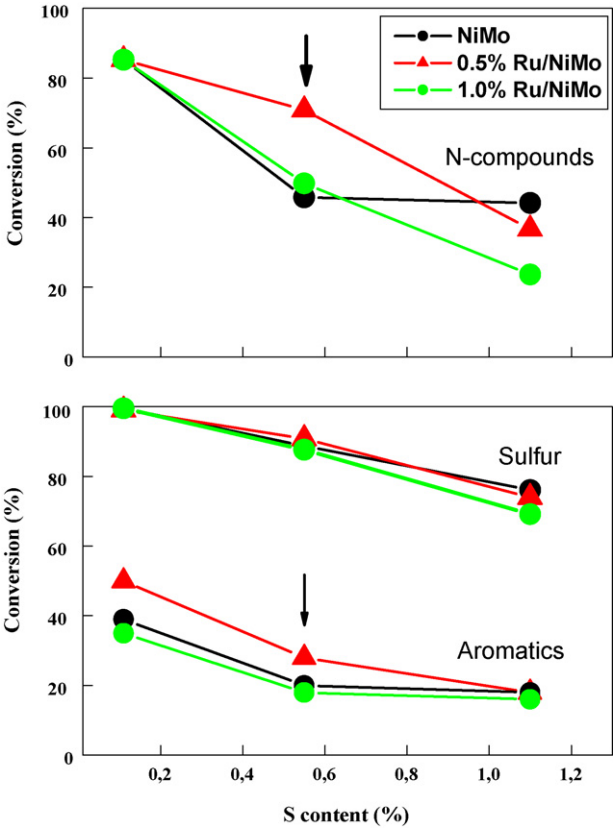

Fig. 4. Influence of total sulfur content in a SRGO on total aromatics, N- and S-compounds conversions at 300 °C (P = 3 MPa, LHSV = 2.2 h^{-1}). The most active catalyst is marked with an arrow.

counterparts based on the NiMo system (data not shown here). This is due to a larger S_{BET} of CoMo/Al_2O_3 with respect to the NiMo/Al_2O_3 reference catalyst (223 vs. 164 $m^2\,g^{-1}$). As expected, the introduction of a second promoter (Pd, Ru) into both commercial catalysts led to a decrease in the catalyst specific surface area, albeit a relatively small one (about 10%) due to a very low loading of Pd(Ru). All the catalysts studied have the same pore diameter (6.6 ± 0.1 nm). The X-ray diffraction (data not shown here) lines for the tetragonal phase of PdO at d-spacing of 0.26, 0.52 and 0.13 nm (ASTM 41-1107) were observed only for the 1.0%Pd/NiMo sample. The crystal size of the PdO phase, as calculated by the Scherrer equation, was ca. 13.7 nm. The diffraction lines of MoO_3 phase, $NiMoO_4$ or Ni(Co)O phases were absent in the diffractograms of all the catalysts, indicating a good dispersion of those phases and/or their amorphous character. Similarly, none of the Ru promoted catalysts shows the formation of RuO_2 crystals, indicating their good dispersion (<4 nm) achieved by very slow controlled calcination in air. This is important because, in general, it was reported that ruthenium oxide tends to be agglomerated during calcination which then results in a decrease in HDS activity of supported RuS_2 [7,24].

An X-ray photoelectron spectroscopy analysis of the NiMo and 0.5%Ru/NiMo catalysts was carried out to investigate the chemical state of the elements and the dispersion of the metal oxide species after catalyst calcination. The binding energy (BE) values corresponding to the Mo $3d_{5/2}$, Ni $2p_{3/2}$ and Ru $3d_{5/2}$ core levels are compiled in Table 2. The BE of Ru $3d_{3/2}$ was not considered because the carbon peak (284.5 eV) overlaps this region. For both catalysts, the BE values for Mo $3d_{5/2}$ and Ni $2p_{3/2}$ regions at 232.5 eV and 856.3 ± 0.1 eV, respectively, strongly suggest the presence of $NiMoO_4$ species [25]. This is in agreement with results

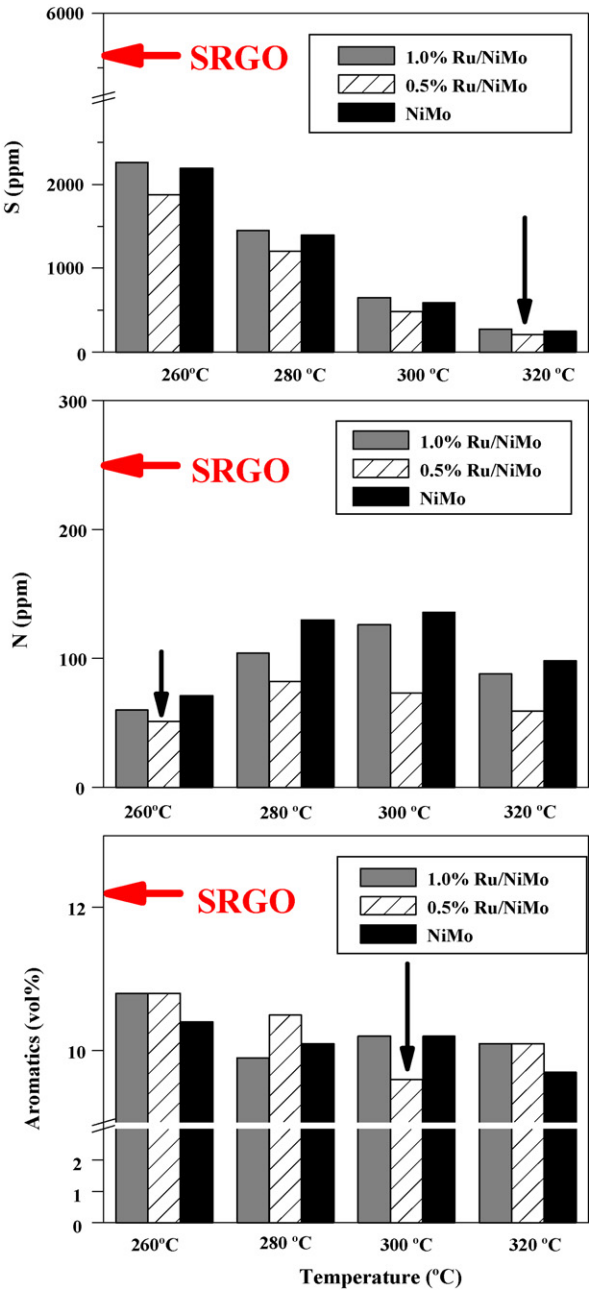

Fig. 5. Effect of Ru-loading and reaction temperature on total S-, N- and aromatics removal in the HDT of SRGO (0.55 wt% of S) over Ru-promoted and unpromoted commercial $NiMo/Al_2O_3$ catalysts. The most active catalyst is marked with an arrow.

found from TPR analysis (*vide infra*). It is noteworthy that the BE value of the Ru $3d_{5/2}$ core level at 281.2 eV, which is indicative of RuO_2 species [26], excluded the electron withdrawn from Mo by Ru, which was previously observed for the $Ru–Mo/Al_2O_3$ catalysts [11]. This is due to the "soft" calcination conditions used in this study (420 °C vs. 600 °C of Ref. [11]), which avoided the formation of Ru–O–Mo species. Finally, a comparison of the Mo/Al atomic ratios in Table 2 indicated that the 0.5%Ru/NiMo catalysts show a larger molybdenum species surface exposure than the Ru-free NiMo reference catalyst. Contrary to the Mo species, the incorporation of Ru into a commercial NiMo catalyst did not alter the surface exposure of the nickel species (see Ni/Al atomic ratio in Table 2).

To explore whether there was some kind of correlation between the reducibility of the oxidic precursors and the activity of the sulfided phases, as already observed earlier [27], temperature-programmed reduction (TPR) profiles of the Ru-promoted NiMo catalysts were recorded (Fig. 6(a)). In good agreement with the literature [28], the TPR profiles of both 0.5%Ru/NiMo and 1.0%Ru/NiMo catalysts show two small peaks in the range 170–280 °C. The detailed study of the Ru/Al_2O_3 systems performed by Goldwasser and co-workers using different complementary techniques indicated that a low temperature peak is associated with a well-dispersed ruthenium phase, while the high temperature peak is related to the reduction of RuO_2 species [28]. The small difference in the reduction temperatures of the RuO_2 phase observed for 0.5Ru%/NiMo and 1.0%Ru/NiMo catalysts (Fig. 6(b)) is most likely due to changes in the crystallite sizes. The H_2-TPR profiles of all catalysts show a broad intense peak with maximum in the range 433–457 °C, which could overlap contributions from the reduction of both NiO and $NiMoO_4$, whereas two reduction steps of the MoO_3 species ($MoO_3 \rightarrow MoO_2 \rightarrow Mo^0$) occurs in the temperature range 550–1050 °C [23,29]. Thus, the formation of a separate Ru phase could be deduced for both Ru-promoted NiMo catalysts (Fig. 6(a)). It is noteworthy that both Ru-containing catalysts record the larger H_2 consumption at higher temperatures due to a spillover effect from the Ru^0 particles.

The effect of Ru incorporation on the surface acid properties of the NiMo reference catalyst was examined by the FTIR of adsorbed pyridine. Fig. 7 shows the infrared spectra of pyridine adsorbed on the calcined NiMo and 0.5%Ru/NiMo catalysts degassed at 450 °C for 2 h. As seen in this figure, both catalysts record strong bands at ca. 1450 and 1540 cm^{-1} arising from pyridine adsorbed on Lewis and Brønsted acid sites, respectively. To obtain the Lewis and Brønsted acid site concentrations, the areas of the corresponding peaks were estimated and their values are shown in Table 3. As seen in this table, both Brønsted and Lewis acid sites are enhanced after Ru incorporation. However, the similar I_{1540}/I_{1450} intensities ratio of both 0.5%Ru/NiMo and NiMo catalysts (0.21 vs. 0.23) indicated the simultaneous increase of both types of acid sites after Ru loading.

To summarize, the characterization of the oxide precursors by a variety of techniques indicated that: (i) Ru addition did not change the morphology of the $NiMo/Al_2O_3$ reference catalyst, (ii) both well-dispersed Ru phase and bulk RuO_2 are formed on the catalyst surface, (iii) the formation of undesirable Ru–O–Mo species was avoided by using controlled "soft" calcination conditions, and (iv) both Brønsted (1540 cm^{-1}) and Lewis (1450 cm^{-1}) acidities are enhanced after Ru addition.

3.4. Characterization of the spent catalysts by XPS

The chemical state of the elements after the HDS of DBT was investigated by the XPS technique. The binding energies (eV) of the core electrons and surface atomic ratios of the spent NiMo and 0.5%Ru/NiMo catalysts are compiled in Table 2. The S 2p energy region of both catalysts showed a single component close to 162.0 eV, which is a characteristic of sulfide (S^{2-}) species. The Ru $3d_{5/2}$ at 280.6 eV is due to RuS_2 [11]. Curve-fitting of the spectra (not shown here) reveals that the principal Mo 3d peak can be broken down into two components: one at about 229.2 ± 0.1 eV due to MoS_2 species [30] and the other at about 232.1 eV associated with non-sulfided Mo species. Similarly to the Mo species, the part of Ni species became unsulfided (probably $NiMoO_4$ phase, as deduced from TPR), as deduced from the BE at ca. 856.5 eV, whereas the peak at about 854.1 eV is due to nickel sulfide species [30]. Considering the percentage of species (given in Table 2 in parentheses), the Ru addition into the NiMo reference catalyst led to an increase in both nickel and molybdenum sulfides.

Table 2
Binding energies (eV) of the core electrons[a] and surface atomic ratios[b] of the oxide precursors and spent Ru/NiMo catalysts tested in the HDS of DBT

Catalyst	Ru $d_{5/2}$[c]	Mo $3d_{5/2}$	Ni $2p_{3/2}$	Ru/Al	Mo/Al	Ni/Al	S/M
NiMo Calcined	–	232.5	856.2	–	0.112	0.043	–
0.5%Ru/NiMo Calcined	281.2	232.6	856.4	0.020	0.147	0.045	–
NiMo Spent (TOS = 5 h)	–	229.2 (81) 232.2 (19)	854.2 (44) 856.6 (20)	–	0.126	0.047	1.19
0.5%Ru/NiMo Spent (TOS = 87 h)	280.6	229.1(90) 232.0(10)	854.1 (49) 856.5 (16)	0.025	0.123	0.048	1.13

[a] Al 2p peak was taken as an internal pattern (BE Al 2p 74.5 eV). The values between parentheses correspond to the percentage of each species (sulfided/non-sulfided).
[b] The atomic factors reported in Ref. [37] were used for the calculation of atomic ratios.
[c] BE of the Ru $3d_{5/2}$ core level was estimated after the deconvolution of the C1s peak.

The similar Mo/Al and Ni/Al atomic ratios of the spent 0.5%Ru/NiMo catalyst (after 87 h on-stream reaction) and NiMo reference catalyst indicate that both catalysts showed similar nickel and molybdenum species surface exposure during on-stream conditions (Table 2). However, the comparison of the Mo/Al atomic ratios of the calcined and spent forms of the 0.5%Ru/NiMo catalysts indicate some decrease in molybdenum species surface exposure during on stream conditions, as deduced from the decrease in the Mo/Al atomic ratio from 0.147 to 0.123. Thus, some sintering of the Mo species might occur during the life test (87 h). Finally, concerning the sulfidation degree of the catalysts studied, the total sulfidation of the components (MoS_2, Ni_3S_2 and RuS_2) should give an S/(Ru + Ni + Mo) atomic ratio of around 1.73. Thus, the experimental value found between 1.13 and 1.19 for all catalysts indicates that sulfidation is not complete.

3.5. Catalyst activity-structure correlation

Taking into account the XRD results, one might deduce that the much better Ru than Pd dispersion might contribute to the better catalytic response of the 1.0%Ru/NiMo catalyst with respect to the 1.0%Pd/NiMo. Several other explanations can be advanced to explain the greater reactivity of the 0.5%Ru/NiMo in both the HDS of DBT and gasoil. Considering the catalyst activity-structure correlation, it may have resulted from (i) hydrogen spillover effect, as deduced from TPR (*vide supra*), (ii) easier sulfidation of the Mo species (Table 2), and (iii) a higher stability of the 0.5%Ru/NiMo catalyst with respect to the NiMo reference catalyst, as confirmed by the life test in the HDS of DBT. Moreover, the positive effect of an increase in the support acidity on overall activity, as a result of the

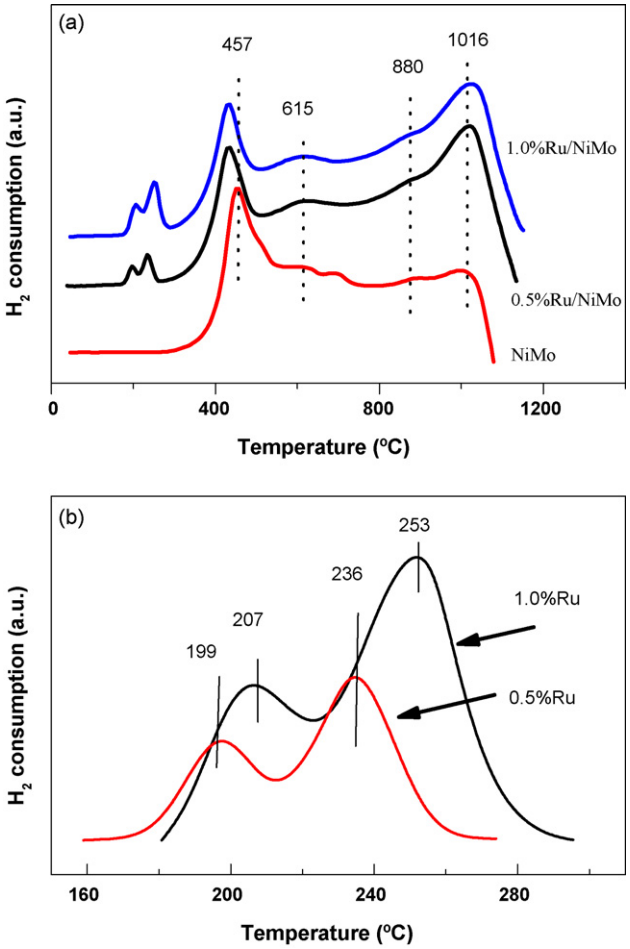

Fig. 6. (a) TPR profiles of unpromoted and Ru-promoted NiMo oxide precursors (b) Influence of Ru loading on the formation of Ru species after calcination at 420 °C.

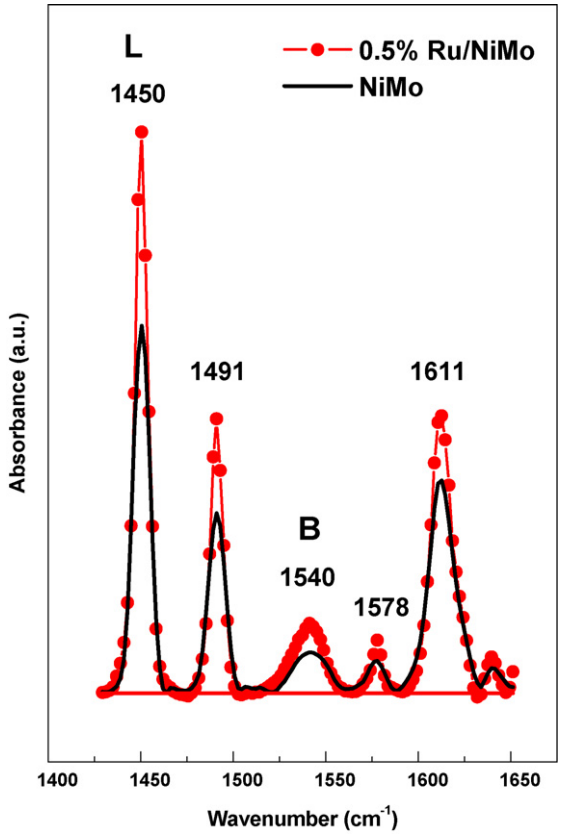

Fig. 7. FTIR spectra of pyridine adsorbed on the oxide NiMo and 0.5%Ru/NiMo precursors.

Table 3
Intensity of the bands (a.u.) in the IR spectra of adsorbed pyridine on the calcined NiMo and 0.5%Ru/NiMo catalysts

Catalyst	I_{1545}	I_{1491}	I_{1450}	I_{1543}/I_{1452}
NiMo	0.481	0.961	2.291	0.21
0.5%Ru/NiMo	0.687	1.194	2.987	0.23

higher number of Brønsted sites for aromatics adsorption, cannot be excluded [31,32]. On the contrary, considering the XPS results of the spent catalysts (*vide supra*), an electronic modification of the NiMo phase by Ru, similar to those reported by Cattenot et al. [10], could be excluded because no shift in the BE values was observed.

From combined TPR and XPS data, the largest hydrogenation properties of the 0.5%Ru/NiMo catalyst are due to the presence of well-dispersed ruthenium sulfide phases on its support surface. This is because the formation of small particles induces some preferential exposed planes, favoring hydrogenation properties, as already mentioned for alumina-supported ruthenium sulfide catalysts [33]. The enhancement of hydrogenation activity on the 0.5%Ru/NiMo catalyst is in agreement with the study by Isoda et al. [16], who proposed that separate RuS_2 phase of sulfided Ru–CoMo/Al_2O_3 catalyst is the site responsible for the selective hydrogenation of 4,6-DMDBT, of which hydrogenated product (having diminished steric hindrance with respect to 4,6-DMDBT) is transferred immediately to the "Co–Mo–S" active sites to be desulfurized [16]. Moreover, the presence of well-dispersed isolated RuS_2 species might contribute to the overall catalytic activity by Ni and Mo sulfides assuming that the RuS_2 species acts as additional active sites for S-atom exchange and/or additional sites for hydrogen dissociation. The ^1H NMR study on the partially desulfurized ruthenium sulfide performed by Lacroix et al. [34] evidenced two H^- and H^+ species: the former led to the formation of –SH groups and the latter being chemisorbed on CUS sites of Ru cations. Thus, assuming that gaseous hydrogen adsorbs dissociatively on the catalyst surface as well as on the isolated RuS_2 species, the hydrogen species consumed in the reaction could be supplemented by means of spillover on the surface [35]. This probably explains the enhanced resistance of the 0.5%Ru/NiMo catalyst to coking with respect to the NiMo reference sample, as demonstrated by the life test in the HDS of DBT.

Finally, concerning the possible positive effect of residual chloride ions on the catalytic response, which was observed for the non-calcined catalysts prepared using $RuCl_3$ [12,36], their contribution, if any, to catalytic activity of 0.5%Ru/NiMo sample should be minimal. Indeed, it was reported that the sulfided RuCoMo/γ–Al_2O_3 catalyst with residual chloride ions on its surface did not record an improved performance in the hydrotreating of atmospheric residual oil with respect to a commercial CoMo/γ–Al_2O_3 reference catalyst [15].

4. Conclusions

The impregnation of a commercial NiMo/γ–Al_2O_3 catalyst with $RuCl_3$ in aqueous solution, followed by slow controlled drying and calcination in air, results in the formation of isolated well-dispersed Ru oxide species, avoiding the formation of undesirable Ru–O–Mo.

In general, the sulfide ternary catalysts based on the NiMo system were found to be more active in the HDS of DBT than those based on CoMo formulation. In this reaction, Ru was more effective as a second promoter than Pd and the optimum Ru content was found to be 0.5 wt%. In the HDS of DBT, this catalyst records the highest hydrogenation properties among the catalysts studied. Consequently, the sulfide 0.5%Ru/NiMo/Al_2O_3 catalyst recorded a better catalytic performance than a commercial NiMo/Al_2O_3 reference catalyst in the simultaneous HDS, HDN and HDA reactions occurring during the hydroprocessing of the SRGO containing 0.55 wt% of S.

Acknowledgements

The authors would like to express their gratitude to Repsol-YPF (Madrid, Spain) for their financial support for this project and permission to publish these results. Comments made by Dr. J.P. Gómez (CTR Repsol-YPF) are gratefully acknowledged.

References

[1] U.S. Environmental Protection Agency, http://ww.epa.gov/otaq/gasoline.htm; http://www.epa.gov/otaq/diesel.htm, 2006.
[2] Europen Union, EU Directive 98/70/EC, 1998.
[3] M.J. Girgis, B.C. Gates, Ind. Eng. Chem. Res. 30 (1991) 2021.
[4] F.L. Plantenga, R.G. Leliveld, Appl. Catal. A: Gen. 248 (2003) 248.
[5] P.T. Vasudevan, J.L.G. Fierro, Catal. Rev. Sci. Eng. 38 (2) (1996) 161.
[6] T.A. Pecoraro, R.R. Chianelli, J. Catal. 67 (1981) 430.
[7] J.A. De los Reyes, Appl. Catal. A: Gen. 322 (2007) 106.
[8] R. Navarro, B. Pawelec, J.L.G. Fierro, P.T. Vasudevan, Appl. Catal. A. Gen. 148 (1996) 23.
[9] B. Pawelec, R.M. Navarro, J.M. Campos-Martin, A. López-Agudo, P.T. Vasudevan, J.L.G. Fierro, Catal. Today 86 (2003) 73.
[10] M. Cattenot, C. Geantet, C. Glasson, M. Breysse, Appl. Catal. A: Gen. 213 (2001) 217.
[11] P.C.H. Mitchell, C.E. Scott, J.-P. Bonnelle, J.G. Grimblot, J. Catal. 107 (1987) 482.
[12] A.S. Hirschon, R.B. Wilson, R.M. Laine, Appl. Catal. 34 (1987) 311.
[13] F.S. Xiao, Q. Xin, X.X. Guo, Appl. Catal. 95 (1993) 21.
[14] I. Mochida, K. Sakanishi, X. Ma, S. Nagao, T. Isoda, Catal. Today 29 (1995) 185.
[15] D.K. Lee, I.C. Lee, S.I. Woo, Appl. Catal. 109 (1994) 195.
[16] T. Isoda, S. Nagao, X. Ma, Y. Korai, I. Mochida, Energy Fuels 10 (2) (1996) 487.
[17] H.S. Joo, J.A. Guin, Fuel Process. Technol. 49 (1996) 137.
[18] X.S. Li, Z.S. Hou, Q. Xin, Stud. Surf. Sci. Catal. 77 (1993) 353.
[19] P. Afanasiev, I. Bezverkhyy, Appl. Catal. A: Gen. 322 (2007) 129.
[20] F. van Looij, P. van der Laan, W.H.J. Stork, D.J. DiCamillo, J. Swain, Appl. Catal. A: Gen. 170 (1998) 1.
[21] T.A. Zepeda, B. Pawelec, J.L.G. Fierro, T. Halachev, J. Catal. 242 (2006) 254.
[22] T.A. Zepeda, B. Pawelec, J.L.G. Fierro, T. Halachev, Appl. Catal. B: Environ. 71 (2007) 223.
[23] T.A. Zepeda, B. Pawelec, J.L.G. Fierro, A. Olivas, S. Fuentes, T. Halachev, Micropor. Mesopor. Mater. 111 (2008) 157.
[24] J.A. De Los Reyes, S. Göbölös, M. Vrinat, M. Breysse, Catal. Lett. 5 (1990) 17.
[25] R. Hernández-Huesca, J. Mérida-Robles, P. Maireles-Torres, E. Rodríguez-Castellón, A. Jiménez-López, J. Catal. 203 (2001) 122.
[26] M. Nagai, K. Koizumi, S. Omi, Catal. Today 35 (1997) 393.
[27] Y.W. Chen, W.C. Hsu, C.S. Lin, B.C. Kang, S.T. Wu, L.J. Leu, J.C. Wu, Ind. Eng. Chem. Res. 29 (1990) 1830.
[28] P. Betancourt, A. Rives, R. Hubaut, C.E. Scott, J. Goldwasser, Appl. Catal. A: Gen. 170 (1998) 307.
[29] R. Nava, R.A. Ortega, G. Alonso, C. Ornelas, B. Pawelec, J.L.G. Fierro, Catal. Today 127 (2007) 70.
[30] P.L. Arias, J.F. Cambra, M.B. Güemez, J.A. Legarreta, B. Pawelec, J.L.G. Fierro, Bull. Soc. Chim. Belg. 104 (4–5) (1995) 197.
[31] S.D. Lin, M.A. Vannice, J. Catal. 143 (1993) 563.
[32] P. Castaño, J.M. Arandes, B. Pawelec, J.L.G. Fierro, A. Gutiérrez, J. Bilbao, Ind. Eng. Chem. Res. 46 (2007) 7417.
[33] J.A. De Los Reyes, M. Vrinat, C. Geantet, M. Breysse, Catal. Today 10 (1991) 645.
[34] M. Lacroix, S. Yuan, M. Breysse, C. Dorémieux-Morin, J. Fraissard, J. Catal. 138 (1992) 409.
[35] E.J.M. Hensen, H.J. Lardinois, V.H.J. de Beer, J.A.R. van Veen, R.A. van Santen, J. Catal. 187 (1999) 95.
[36] G. Muralidhar, F.E. Massoth, J. Shabtai, J. Catal. 85 (1984) 44.
[37] C.D. Wagner, W.M. Riggs, L.E. Davis, J.F. Moulder, G.E. Muilenberg, Handbook of X-ray Photoelectron Spectroscopy, Perkin Elmer Corp., 1979.